

Heat Convection Between Two Confocal Elliptic Tubes Placed at Different Orientations

F. M. Mahfouz¹ and H. M. Badr^{2,*}

¹ Department of Mechanical Engineering, University of Engineering & Technology, Taxila, Pakistan

² Department of Mechanical Engineering, King Fahd University of Petroleum & Minerals, KFUPM Box #322, Dhahran, Saudi Arabia

Received 02 April 2009; Accepted (in revised version) 24 June 2009

Available online 30 July 2009

Abstract. In this paper, transient and steady natural convection heat transfer in an elliptical annulus has been investigated. The annulus occupies the space between two horizontal concentric tubes of elliptic cross-section. The resulting velocity and thermal fields are predicted at different annulus orientations assuming isothermal surfaces. The full governing equations of mass, momentum and energy are solved numerically using the Fourier Spectral method. The heat convection process between the two tubes depends on Rayleigh number, Prandtl number, angle of inclination of tube axes and the geometry and dimensions of both tubes. The Prandtl number and inner tube axis ratio are fixed at 0.7 and 0.5, respectively. The problem is solved for the two Rayleigh numbers of 10^4 and 10^5 considering a ratio between the two major axes up to 3 while the angle of orientation of the minor axes varies from 0 to 90° . The results for local and average Nusselt numbers are obtained and discussed together with the details of both flow and thermal fields. For isothermal heating conditions, the study has shown an optimum value for major axes ratio that minimizes the rate of heat transfer between the two tubes. Another important aspect of this paper is to prove the successful use of the Fourier Spectral Method in solving confined flow and heat convection problems.

AMS subject classifications: 80A20, 35Q80

Key words: Heat convection, Elliptic tubes, Fourier spectral methods, Rayleigh number, Prandtl number.

1 Introduction

As it has been the case for fundamental engineering problems, natural convection in an annular enclosure has been the target of persistent scientific research. The research

*Corresponding author.

URL: <http://www.kfupm.edu.sa/me/faculty/badrhm.htm>

Email: badrhm@kfupm.edu.sa (H. M. Badr)

has been directed to this problem because of its pertinence to many practical engineering applications. These applications include nuclear reactor systems, thermal storage and solar heating systems. The annular space can be geometrically formed by the region between either concentric or eccentric two elliptical tubes. The concentric elliptical tube geometry can represent different annuli configurations ranging from the annulus formed between two concentric circular tubes to annulus formed by a flat plate surrounded by an elliptical tube. In case of annulus formed between two concentric, confocal elliptic tubes, the geometry of the annulus is controlled by two parameters. These are the ratio of the major axis of outer tube to the major axis of inner tube and the axis ratio of both tubes.

The problem of steady natural convection in a horizontal annulus between two concentric/eccentric circular tubes was considered by many researchers. The work of Kuehn and Goldstein [1] comes in the vanguard, with pioneering experimental and theoretical results and with good, thorough literature review. The results in that work covered the most details of steady heat transfer characteristics and flow patterns developed in the annulus. The heat transfer results were presented in terms of Nusselt number and equivalent conductivity. The equivalent conductivity is defined as the actual heat flux divided by the heat flux that would occur by pure conduction. The authors have further extended their experimental study [2] to include the natural convection in an eccentric circular annulus; the case which has been considered later by a number of researchers [3–10].

In comparison with the circular concentric and eccentric cases, a few number of studies were conducted on natural convection in a non-circular enclosures such as the elliptic annulus considered in this study. Lee and Lee [11] have investigated experimentally and theoretically, through a few test cases, steady natural convection of air in a symmetric annulus formed between two concentric, confocal elliptic tubes. They used the conventional finite-difference method to solve the governing equations that were written in stream function-vorticity formulation. Their numerical results were verified through comparisons with the experimental results performed using the Mach-Zehnder interferometer and smoke flow visualization. Elshamy et al. [12] used the finite-volume approach to investigate numerically the steady natural convection in horizontal symmetric annulus formed between two confocal elliptic tubes. They presented the results in terms of the local and average Nusselt numbers together with correlations for the average Nusselt number.

In their numerical investigation to study the steady natural convection in some horizontal concentric and eccentric elliptical configurations, Cheng and Chao [13] used the finite-volume discretization technique method to solve the governing equations that were written in terms of primitive variables. They discretized the governing equations using a curvilinear grid system that was generated by a body-fitted coordinate transformation method. They presented their heat transfer results for a number of different symmetrical elliptic configurations, expressing their results in terms of equivalent conductivity.

Zhu et al. [14] used the Differential Quadrature (DQ) method to study numerically

the steady natural convection in a number of symmetrical elliptic annuli configurations. The governing equations written in stream function-vorticity formulation were transformed from physical Cartesian domain to computational domain using an analytical function. The authors have showed that the DQ method is capable of producing accurate numerical solutions with small number of mesh points.

The above literature review shows that the previous studies on elliptic enclosures have focused mainly on steady natural convection problems and in case of symmetric configurations. The only attempt to investigate the case of asymmetric elliptic enclosure was made by Schreiber and Singh [15]. In that study, they investigated natural convection in a horizontal elliptic annulus placed at different orientation with respect to gravity vector. They used the Fourier series expansion method to reduce the governing PDE into ODE and then employed a package that was designed to solve the ODE through finite element collocation method. Their study, however, focused on the special case of steady natural convection from a flat plate surrounded by an elliptical tube. The lack of detailed information, especially those related to the effect of annulus orientation and major axes ratio, on the transient and steady heat transfer and fluid flow in an asymmetric annulus formed between two confocal elliptic tubes was the first motivation for this study. On the other hand, the Fourier Spectral Method (FSM) has been used very successfully in solving heat transfer/fluid flow problems associated with unconfined flow regimes. However, the method has not been used, to the best of authors' knowledge, in tackling the confined flow associated problems. So, the second motivation for this study was to examine the suitability of the FMS in handling confined heat convection/fluid flow associated problems.

2 Problem formulation

The annulus geometry, shown in Fig. 1, is the two-dimensional space sandwiched between two confocal, concentric elliptical horizontal tubes. The tubes are long enough to create a two-dimensional velocity and thermal fields. The minor axes of the two elliptic tubes are aligned and oriented at an arbitrary angle, λ , with respect to the gravity vector. The temperature of the inner surface of the annulus is kept uniform at T_i while that of the outer surface is kept uniform at T_o ($T_o < T_i$). The resulting buoyancy driven flow of the boussinesq fluid that fills the annulus is assumed to be laminar and two dimensional. The equations of conservation of mass, momentum and energy can be written in Cartesian coordinates in terms of stream function, vorticity and temperature as follows:

$$\frac{\partial \zeta'}{\partial \tau} + \frac{\partial \psi'}{\partial y'} \frac{\partial \zeta'}{\partial x'} - \frac{\partial \psi'}{\partial x'} \frac{\partial \zeta'}{\partial y'} = \nu \left(\frac{\partial^2 \zeta'}{\partial x'^2} + \frac{\partial^2 \zeta'}{\partial y'^2} \right) + \frac{1}{\rho} \left(\frac{\partial F_{y'}}{\partial x'} - \frac{\partial F_{x'}}{\partial y'} \right), \quad (2.1)$$

$$\zeta' + \frac{\partial^2 \psi'}{\partial x'^2} + \frac{\partial^2 \psi'}{\partial y'^2} = 0, \quad (2.2)$$

$$\frac{\partial T}{\partial \tau} + \frac{\partial \psi'}{\partial y'} \frac{\partial T}{\partial x'} - \frac{\partial \psi'}{\partial x'} \frac{\partial T}{\partial y'} = \frac{k}{\rho c} \left(\frac{\partial^2 T}{\partial x'^2} + \frac{\partial^2 T}{\partial y'^2} \right), \quad (2.3)$$

where τ is the time, ρ is the density, ν is the kinematics viscosity, k is the thermal conductivity and c is the specific heat. ψ' is the stream function, ζ' is the vorticity, T is the temperature and

$$F_{x'} = \rho g \beta (T - T_0) \sin(\lambda), \quad F_{y'} = \rho g \beta (T - T_0) \cos(\lambda),$$

are the components of the buoyancy force F_b .

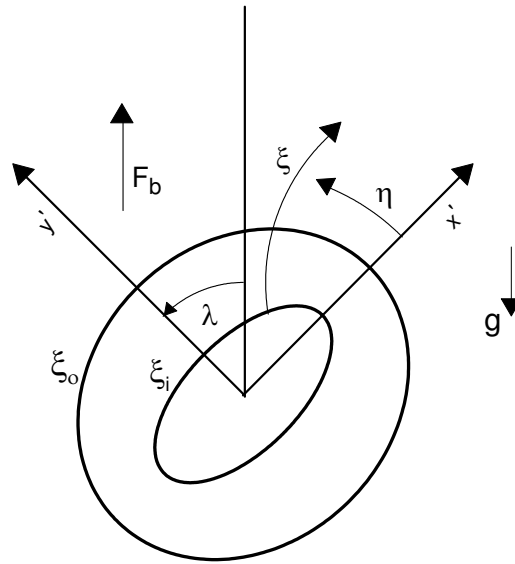


Figure 1: Physical domain and coordinate system.

The steady flow and thermal fields in the annular space between the two tubes are obtained by studying the time-development of both fields starting from a well-defined initial condition until reaching the steady state. At time $t=0$, the inner surface is assumed to be suddenly heated to a temperature T_i , while the outer surface temperature is kept unchanged at T_0 . The fluid in the annulus is initially at rest and at the same uniform temperature, T_0 , of outer wall. The boundary conditions are the impermeability and no-slip condition together with the uniform temperature at the inner and outer surfaces. These boundary conditions can be expressed mathematically as follows:

$$\frac{\partial \psi'}{\partial x'} = 0, \quad \frac{\partial \psi'}{\partial y'} = 0, \quad \text{and } T = T_i, \quad \text{on the inner surface,} \quad (2.4a)$$

$$\psi' = \frac{\partial \psi'}{\partial x'} = 0, \quad \frac{\partial \psi'}{\partial y'} = 0, \quad \text{and } T = T_0, \quad \text{on the outer surface.} \quad (2.4b)$$

Let us introduce the following dimensionless variables,

$$\begin{aligned}
 x &= \frac{x'}{a_i}, & y &= \frac{y'}{a_i}, & t &= \frac{\tau\alpha}{a_i^2}, \\
 \psi &= \frac{\psi'}{\alpha}, & \zeta &= -\zeta' \frac{a_i^2}{\alpha}, & \phi &= \frac{T - T_o}{T_i - T_o},
 \end{aligned}$$

where a_i is the length of semi-major axis of the inner tube and α is the thermal diffusivity of the fluid. In order to prepare the governing equations to be tackled by Fourier Spectral method, lets us also introduce the elliptic coordinates (ζ, η) defined as

$$x = d \cosh(\zeta) \cos(\eta), \quad y = d \sinh(\zeta) \sin(\eta),$$

where $(d=d'/a_i)$ is the dimensionless focal distance. The use of the above orthogonal coordinates has the privilege of expressing the boundary conditions along coordinate lines without the need of interpolation. The governing equations can now be written in the elliptic coordinates as:

$$\begin{aligned}
 \frac{\partial \zeta}{\partial t} &= \text{Pr} \left(\frac{\partial^2 \zeta}{J \partial \zeta^2} + \frac{\partial^2 \zeta}{J \partial \eta^2} \right) + \frac{\partial \psi}{J \partial \zeta} \frac{\partial \zeta}{\partial \eta} - \frac{\partial \psi}{J \partial \eta} \frac{\partial \zeta}{\partial \zeta} \\
 &+ \frac{dRa \text{Pr}}{8} (\cosh \zeta \sin \eta \sin \lambda - \sinh \zeta \cos \eta \cos \lambda) \frac{\partial \phi}{J \partial \zeta} \\
 &+ \frac{dRa \text{Pr}}{8} (\sinh \zeta \cos \eta \sin \lambda + \cosh \zeta \sin \eta \cos \lambda) \frac{\partial \phi}{J \partial \eta}, \tag{2.5}
 \end{aligned}$$

$$\zeta = \frac{\partial^2 \psi}{J \zeta^2} + \frac{\partial^2 \psi}{J \partial \eta^2}, \tag{2.6}$$

$$\frac{\partial \phi}{\partial t} = \left(\frac{\partial^2 \phi}{J \partial \zeta^2} + \frac{\partial^2 \phi}{J \partial \eta^2} \right) + \frac{\partial \psi}{J \partial \zeta} \frac{\partial \phi}{\partial \eta} - \frac{\partial \psi}{J \partial \eta} \frac{\partial \phi}{\partial \zeta}, \tag{2.7}$$

where

$$J = d^2(\cosh^2 \zeta - \cos^2 \eta),$$

is the determinant of the Jacobian of coordinate transformation matrix,

$$Ra = \frac{g\beta}{\nu\alpha} (2a_i)^3 (T_i - T_o),$$

is the Rayleigh number and $\text{Pr}=\nu/\alpha$ is the Prandtl number.

The velocity components in ζ and η direction are related to the stream function by

$$V_\zeta = \frac{1}{J^{\frac{1}{2}}} \frac{\partial \psi}{\partial \eta}, \quad V_\eta = -\frac{1}{J^{\frac{1}{2}}} \frac{\partial \psi}{\partial \zeta}.$$

In the new variables, the initial condition for the temperature of the stagnant fluid inside the annulus at times $t \leq 0$ is $\phi=0$ that is exactly the same as that of the outer

surface. At the start of computations ($t=0$) the inner surface of the annulus assumes a sudden temperature rise to $\phi=1$ and from that moment the time development of both flow and thermal fields starts.

The boundary conditions (2.4) can now be expressed as

$$\frac{\partial \psi}{\partial \xi} = 0, \quad \frac{\partial \psi}{\partial \eta} = 0, \quad \text{and} \quad \phi = 1, \quad \text{at} \quad \xi = \xi_i, \quad (2.8a)$$

$$\psi = \frac{\partial \psi}{\partial \xi} = 0, \quad \frac{\partial \psi}{\partial \eta} = 0, \quad \text{and} \quad \phi = 0, \quad \text{at} \quad \xi = \xi_o, \quad (2.8b)$$

where ξ_i defines the inner tube surface ($= \tanh^{-1} Ar_i$) while ξ_o defines the outer tube surface ($= \tanh^{-1} Ar_o$),

$$Ar_i = \sqrt{1 - (1 - Ar_o^2) \times Mr^2},$$

Mr is the outer to inner tube major axes ratio ($= a_o/a_i$).

3 The Method of solution

The method used for solving the governing equations (2.5)-(2.7) to obtain the time development of both velocity and thermal fields is based on approximating the stream function, vorticity and temperature using Fourier series expansion. The approach is similar to that used by Badr and Dennis [16]. The stream function ψ , vorticity ζ and temperature ϕ are now approximated as

$$\psi(\xi, \eta, t) = \frac{1}{2} F_o(\xi, t) + \sum_{n=1}^N \left(f_n(\xi, t) \sin(n\eta) + F_n(\xi, t) \cos(n\eta) \right), \quad (3.1a)$$

$$\zeta(\xi, \eta, t) = \frac{1}{2} G_o(\xi, t) + \sum_{n=1}^N \left(g_n(\xi, t) \sin(n\eta) + G_n(\xi, t) \cos(n\eta) \right), \quad (3.1b)$$

$$\phi(\xi, \eta, t) = \frac{1}{2} H_o(\xi, t) + \sum_{n=1}^N \left(h_n(\xi, t) \sin(n\eta) + H_n(\xi, t) \cos(n\eta) \right), \quad (3.1c)$$

where $F_o, f_n, F_n, G_o, g_n, G_n, H_o, h_n$ and H_n are the Fourier coefficients and N represents the number of terms considered in the Fourier series. Substitution of ψ, ζ and ϕ defined in (3.1a)-(3.1c) in Eqs. (2.5)-(2.7) results in the following set of differential equations:

$$\frac{\partial^2 F_o}{\partial \xi^2} = \frac{d^2}{2} (\cosh 2\xi G_o - G_2), \quad (3.2a)$$

$$\frac{\partial^2 f_n}{\partial \xi^2} - n^2 f_n = \frac{d^2}{2} \left(\cosh 2\xi g_n - \frac{1}{2} [g_{(n+2)} + \text{sgn}(n-2)g_{|n-2|}] \right), \quad (3.2b)$$

$$\frac{\partial^2 F_n}{\partial \xi^2} - n^2 F_n = \frac{d^2}{2} \left(\cosh 2\xi G_n - \frac{1}{2} [\delta_{n2} G_o + G_{(n+2)} + G_{|n-2|}] \right), \quad (3.2c)$$

$$d^2 \left(\cosh 2\zeta \frac{\partial G_o}{\partial t} - \frac{\partial G_2}{\partial \zeta} \right) = 2 \text{Pr} \frac{\partial^2 G_o}{\partial \zeta^2} + S_o(\zeta, t), \tag{3.3a}$$

$$d^2 \left[\cosh 2\zeta \frac{\partial g_n}{\partial t} - \frac{1}{2} \left(\frac{\partial g_{(n+2)}}{\partial t} + \text{sgn}(n-2) \frac{\partial g_{|n-2|}}{\partial t} \right) \right] \\ = 2 \text{Pr} \left(\frac{\partial^2 g_n}{\partial \zeta^2} - n^2 g_n \right) + n F_n \frac{\partial G_o}{\partial \zeta} - n G_n \frac{\partial F_o}{\partial \zeta} + S_{n1}(\zeta, t), \tag{3.3b}$$

$$d^2 \left[\cosh 2\zeta \frac{\partial G_n}{\partial t} - \frac{1}{2} \left(\delta_{n2} \frac{\partial G_o}{\partial t} + \frac{\partial g_{(n+2)}}{\partial t} + \frac{\partial g_{|n-2|}}{\partial t} \right) \right] \\ = 2 \text{Pr} \left(\frac{\partial^2 G_n}{\partial \zeta^2} - n^2 G_n \right) - n f_n \frac{\partial G_o}{\partial \zeta} + n g_n \frac{\partial F_o}{\partial \zeta} + S_{n2}(\zeta, t), \tag{3.3c}$$

$$d^2 \left(\cosh 2\zeta \frac{\partial H_o}{\partial t} - \frac{\partial H_2}{\partial \zeta} \right) = 2 \frac{\partial^2 H_o}{\partial \zeta^2} + Z_o(\zeta, t), \tag{3.4a}$$

$$d^2 \left[\cosh 2\zeta \frac{\partial h_n}{\partial t} - \frac{1}{2} \left(\frac{\partial h_{(n+2)}}{\partial t} + \text{sgn}(n-2) \frac{\partial h_{|n-2|}}{\partial t} \right) \right] \\ = 2 \left(\frac{\partial^2 h_n}{\partial \zeta^2} - n^2 h_n \right) + n F_n \frac{\partial H_o}{\partial \zeta} - n H_n \frac{\partial F_o}{\partial \zeta} + Z_{n1}(\zeta, t), \tag{3.4b}$$

$$d^2 \left[\cosh 2\zeta \frac{\partial H_n}{\partial t} - \frac{1}{2} \left(\delta_{n2} \frac{\partial H_o}{\partial t} + \frac{\partial h_{(n+2)}}{\partial t} + \frac{\partial h_{|n-2|}}{\partial t} \right) \right] \\ = 2 \left(\frac{\partial^2 H_n}{\partial \zeta^2} - n^2 H_n \right) - n f_n \frac{\partial H_o}{\partial \zeta} + n h_n \frac{\partial F_o}{\partial \zeta} + Z_{n2}(\zeta, t), \tag{3.4c}$$

where $S_o, S_{n1}, S_{n2}, Z_o, Z_{n1}$ and Z_{n2} are all easily identifiable functions. Eqs. (3.2a)-(3.4c) define $(6N + 3)$ differential equations that should be solved simultaneously at every time step to get the details of the flow and thermal fields. The initial and boundary conditions for all Fourier functions presented in Eqs. (3.2)-(3.4) are deduced from (2.8) and can be expressed as:

$t = 0$: at $\zeta = \zeta_i$,

$$F_n = f_n = \frac{\partial F_n}{\partial \zeta} = \frac{\partial f_n}{\partial \zeta} = \frac{\partial F_o}{\partial \zeta} = 0, \quad H_n = h_n, \quad \text{and} \quad H_o = 2, \tag{3.5a}$$

and for $\zeta_i < \zeta \leq \zeta_0$,

$$\left[\frac{\partial F_o}{\partial \zeta}, F_n, \frac{\partial F_n}{\partial \zeta} \right] = 0, \quad f_n = \frac{\partial f_n}{\partial \zeta} = 0, \quad G_o = G_n = g_n, \\ \text{and} \quad H_o = H_n = h_n = 0, \tag{3.5b}$$

$t > 0$: at $\zeta = \zeta_i$

$$F_n = f_n = \frac{\partial F_n}{\partial \zeta} = \frac{\partial f_n}{\partial \zeta} = \frac{\partial F_o}{\partial \zeta} = 0, \quad H_o = 2, \quad H_n = h_n = 0, \tag{3.5c}$$

and at $\zeta = \zeta_0$,

$$F_n = f_n = \frac{\partial F_n}{\partial \zeta} = \frac{\partial f_n}{\partial \zeta} = \frac{\partial F_o}{\partial \zeta} = 0, \quad \text{and} \quad H_o = H_n = h_n = 0. \tag{3.5d}$$

Integrating both sides of Eq. (3.2a) with respect to ζ between $\zeta=\zeta_i$ and $\zeta=\zeta_o$ and using the boundary conditions in Eq. (3.5) gives the following integral condition:

$$\int_{\zeta_i}^{\zeta_o} \frac{d^2}{2} (\cosh 2\zeta G_o - G_2) d\zeta = 0. \quad (3.6a)$$

Similarly, multiplying both sides of Eqs. (3.2b) and (3.2c) by $e^{-n\zeta}$ and integrating from $\zeta=\zeta_i$ to $\zeta=\zeta_o$ and using boundary conditions (3.5), one can obtain the following integral conditions

$$\int_{\zeta_i}^{\zeta_o} \frac{d^2}{2} \left(\cosh 2\zeta g_n - \frac{1}{2} [g_{(n+2)} + \operatorname{sgn}(n-2)g_{|n-2|}] \right) e^{-n\zeta} d\zeta = 0, \quad (3.6b)$$

$$\int_{\zeta_i}^{\zeta_o} \frac{d^2}{2} \left(\cosh 2\zeta G_n - \frac{1}{2} [\delta_{n2}G_n + G_{(n+2)} + G_{|n-2|}] \right) e^{-n\zeta} d\zeta = 0, \quad (3.6c)$$

where $\delta_{n2}=1$ if $n=2$ and $\delta_{n2}=0$ if $n \neq 2$.

The above integral conditions are used at every time step to calculate the values of the functions G_o , g_n and G_n on the inner tube surface ($\zeta=\zeta_i$). These functions are then used to predict the vorticity distribution at the inner tube surface. The vorticity distribution at outer wall is calculated from the same three functions but calculated at the outer wall ($\zeta=\zeta_o$).

Assume that the number of points in the ζ direction is N_p that makes a grid size equal to $(\zeta_o - \zeta_i)/(N_p - 1)$. The value of N_p is taken as 101 in the low Ra cases and increases with the increase of Ra until reaching 181 at $Ra=10^5$. The number of terms in Fourier series is taken as 5 terms at the start of computations and then more terms are added as time increases until reaching steady state. The maximum number of terms used in most cases is 40. The solution procedure is the same as that described by Badr and Dennis [16] and Mahfouz and Badr [17]. The only difference is the presence of the unknown terms $g_{(n+2)}$, and $H_{(n+2)}$ in Eqs. (3.3)-(3.6). These terms were first approximated and corrected through an iterative procedure at every time step.

After obtaining the stream function and temperature distributions, the flow velocities and heat transfer characteristics can be easily determined. The heat transfer results can be presented in terms of either the equivalent conductivity or the Nusselt number. The former will be considered for comparisons with previous works while the latter will be used to present the heat transfer results in this study.

The local Nusselt numbers at the inner and outer surfaces of the annulus are defined as

$$Nu_i = \frac{h_i L_i}{k}, \quad Nu_o = \frac{h_o L_o}{k}, \quad (3.7)$$

where k is the fluid thermal conductivity and L_i and L_o are characteristic lengths related to the inner and outer walls, h_i and h_o are the local heat transfer coefficients at

both walls and are defined as:

$$h_i = \frac{\dot{q}_i}{T_i - T_o}, \quad \dot{q}_i = -k\left(\frac{\partial T}{\partial s_n}\right)_i,$$

$$h_o = \frac{\dot{q}_o}{T_i - T_o}, \quad \dot{q}_o = -k\left(\frac{\partial T}{\partial s_n}\right)_o,$$

where \dot{q} is the rate of heat transfer per unit area, S_n is the normal direction to the surface. From the above definitions one can deduce

$$Nu_i = -\frac{L_i}{a_i} \left(J^{-\frac{1}{2}} \frac{\partial \phi}{\partial \xi} \right)_i, \quad Nu_o = -\frac{MrL_o}{a_o} \left(J^{-\frac{1}{2}} \frac{\partial \phi}{\partial \xi} \right)_o, \quad (3.8)$$

where

$$J = d^2(\cosh^2 \xi - \cos^2 \eta).$$

The average Nusselt number is defined as

$$\overline{Nu} = \frac{1}{P} \int_0^P Nu dP,$$

where P is the perimeter of the elliptic section. Taking the characteristic lengths L_i and L_o as P_i/π and P_o/π respectively, the average Nusselt number at inner and outer surfaces can be expressed as:

$$\overline{Nu}_i = -\left(\frac{\partial H_o}{\partial \xi} \right)_i, \quad \overline{Nu}_o = -\left(\frac{\partial H_o}{\partial \xi} \right)_o. \quad (3.9)$$

The energy balance in the steady state entails that the heat transfer through the annulus from the inner surface should be equal to that dissipated to the surrounding from the outer surface. The above definitions for local and average Nusselt numbers are taken deliberately to express this fact. That is the average values of Nu_i and Nu_o should be equal when reaching the steady state.

4 Accuracy of the numerical solution

In order to validate the method of solution and the numerical technique, numerical results were first obtained for some special cases and then compared with the corresponding data previously reported in the literature. The case of natural convection within a concentric annulus with geometric parameters $Ar_i=0.998$, and $Mr=2.6$ and filled with air ($Pr=0.7$) at $Ra=1.95 \times 10^4$ and $Ra=9.75 \times 10^4$ is considered for comparison. The results are presented in Figs. 2 and 3 and compared with the earlier data reported by Kuehn and Goldstein [1] and Cheng and Chao [13]. The present results for streamlines and isotherms patterns, as shown in Fig. 2 are in very good agreement with the corresponding ones of Kuehn and Goldstein [1]. The results for local equivalent conductivity distribution on inner and outer surfaces, which are presented in Fig. 3 together with that of Kuehn and Goldstein [1] and Cheng and Chao [13], are also in good agreement.

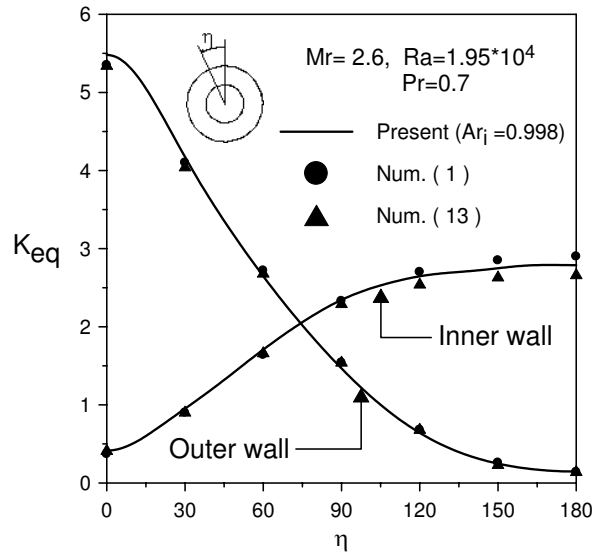


Figure 3: Equivalent conductivity distribution at inner and outer walls of concentric circular annulus and comparison with Refs. [1, 13].

lating crescent-shaped eddies, one on each half of the annulus. Each eddy is formed of a flow current moving upward near to the inner surface and downward near of outer surface. The streamline, separating the two circulating eddies, passes through two separation points and two stagnation points. One of the two separation points is located at the top of inner surface at $\eta=0$ and the other at the bottom of outer surface at $\eta=180^\circ$. One the other hand, one of the two stagnation points is located at the top of outer surface at $\eta=0$ and the other at the bottom of inner surface at $\eta=180^\circ$.

At small time, $t=0.05$, Fig. 4a shows a newborn buoyancy driven eddy in the right side circulating with its center close to the inner surface. At this stage, the induced circulating flow is very weak as can be inferred from the small values of the stream function as well as from the small values of tangential velocity plotted in Fig. 5. At this stage, the heat transfer rate from the inner surface is very high as a result of high temperature difference between the inner surface and the adjacent fluid. The heat transfer through the annulus in that early stage is dominated by heat conduction within a very thin thermal layer in the vicinity of the inner tube surface. Such a mode has been called pseudo-conduction by Grigull and Hauf [18] as cited by Kuehn and Goldstein [1]. The domination of conduction is reflected in the shape of isotherms which appear as almost elliptic loops encircling the inner tube surface. At this time stage, the temperature gradient at $\eta=0$ close to the inner surface is very high while having very low values at the outer surface as depicted from Fig. 6. At time $t=0.1$ (Fig. 4b), the conduction mode of heat transfer is still dominating but with more effect of convection currents which increase the maximum value of stream function. At that time, the values of V_η near both inner and outer surfaces increase as shown in Fig. 5 signaling an increasing effect of convection currents causing some deflection in the isotherms at

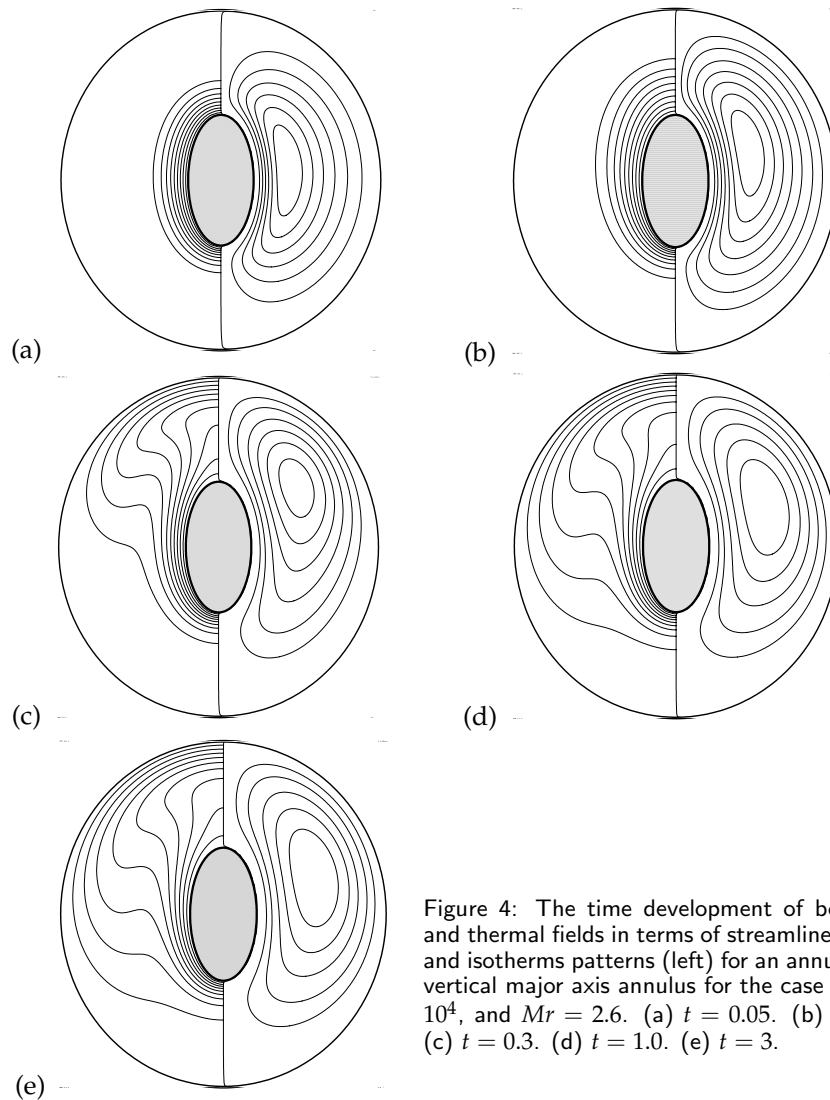


Figure 4: The time development of both flow and thermal fields in terms of streamlines (right) and isotherms patterns (left) for an annulus with vertical major axis annulus for the case of $Ra = 10^4$, and $Mr = 2.6$. (a) $t = 0.05$. (b) $t = 0.1$. (c) $t = 0.3$. (d) $t = 1.0$. (e) $t = 3$.

the upper zone where the thermal plume formation is expected. With further increase in time, $t=0.3$ (Fig. 4c), the upward circulating flow is clearly intensified in the upper region with more increase in the values of the stream function than those at $t=0.05$ and 0.1 . This was accompanied with upward shifting of the eddy center and with clear developing of thermal plume in the upper zone of the annulus. In the thermal plume region, the isotherms are highly condensed near the top of the outer surface which indicates higher temperature gradient (see Fig. 6) and so higher rates of heat transfer. With further increase of time to $t=1$ (Fig. 4d) the flow and thermal fields become closer to the steady state which is almost reached at $t=3$ (Fig. 4e). At this steady state, the flow field becomes strongly circulating and the thermal field becomes established

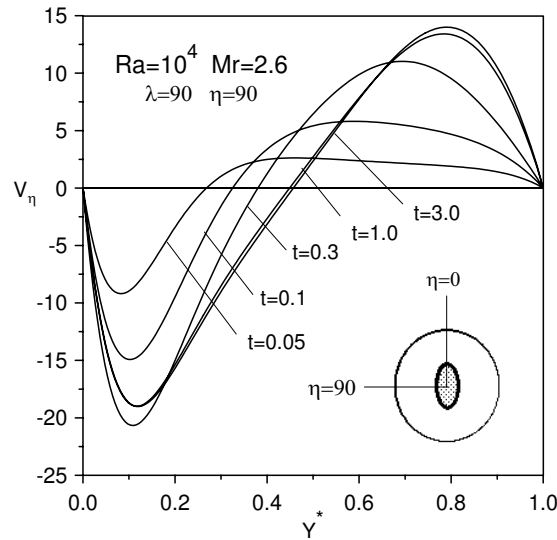


Figure 5: The V_η distribution along the minor axis, $\eta = 90^\circ$ at different times.

with a clear thermal plume in the upper part of the annulus.

Fig. 7 shows the distribution of local Nusselt number at the annulus inner surface (Fig. 7a) and outer surface (Fig. 7b) for the same above case and at the same times. It can be seen from Fig. 7a that at small time, $t = 0.05$, Nu has relatively higher values at all points of the inner surface with the highest at the bottom end. This reflects high heat transfer rate from the entire inner surface of the annulus at that early stage. It also reflects the effect the convection currents which, though very weak, cause an increase in heat transfer at the lower stagnation point of the inner tube. At that early time, the

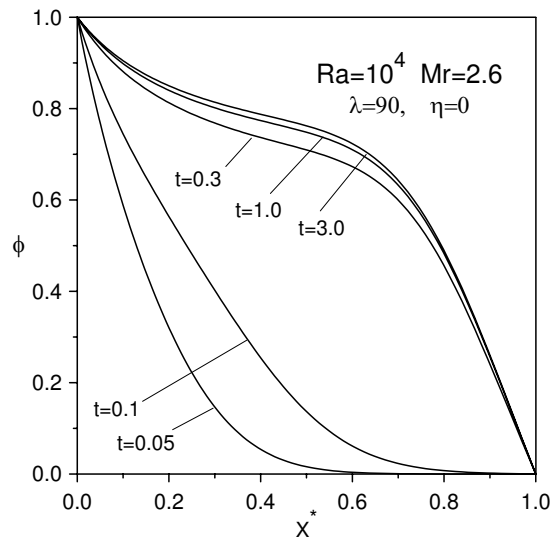


Figure 6: The temperature distribution along the major axis, $\eta = 0$ at different times.

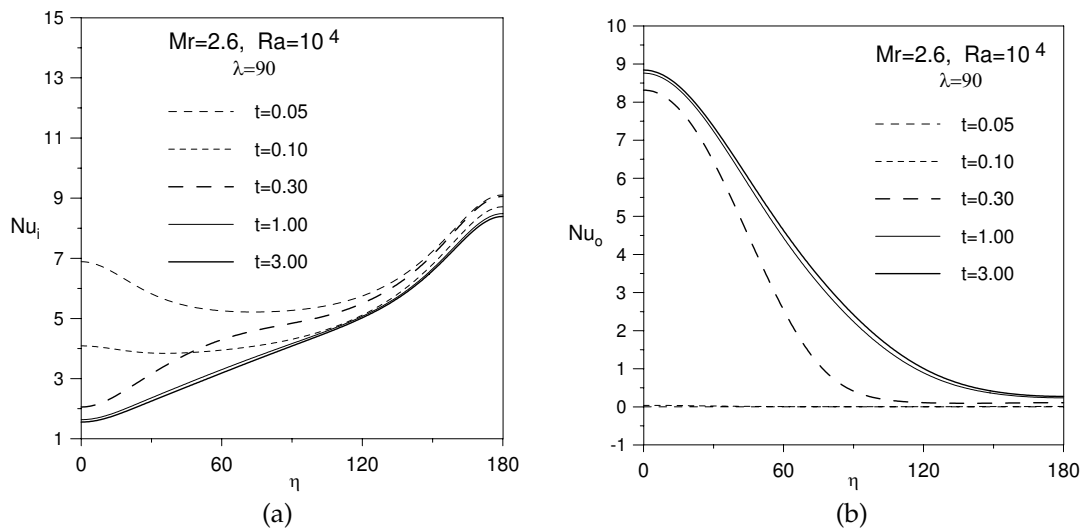


Figure 7: The time development of Nusselt number distribution along (a) the inner surface and along (b) the outer surface for the vertical case at $Ra = 10^4$ and $Mr = 2.6$.

thermal layer has been initiated in the vicinity of the inner wall surface but has not yet reached the outer wall, indicating zero heat transfer and accordingly zero Nu at that surface. As time increases to $t=0.3$, the Nusselt number distribution along the inner surface is still characterized by higher values at $\eta=180^\circ$ and lower values at $\eta=0$ but with further decrease at all points which declares a reduction in heat rates from inner surface as a result of thicker thermal layer. Meanwhile, the situation at the outer wall surface becomes different since the thermal boundary layer has already reached the outer surface and heat is dissipating from that surface at higher rates especially in the thermal plume region. In the lower part of the annulus near the outer surface, the fluid is almost stagnant causing small heat transfer rates and so very small values of Nu_o . At $t=1$, the flow and thermal fields are approaching steady state with intensive convective flow currents emanating upward vigorously and impinging the outer wall at the uppermost vertical part of the annulus, causing a clear thermal plume in that region.

The time development of \overline{Nu} at the inner and outer surfaces is shown in Figs. 8a-d for the case of vertical annulus when $Ra=10^4$ and for different major axes ratios. The time developments of \overline{Nu} at the inner and outer surfaces for the case of pure conduction regime are shown in the same figures. The transient conduction solution is obtained by solving the energy equation with convection terms set to zeros. The figure shows that the time variation of \overline{Nu}_i at inner surface is generally similar to that for elliptic tube placed in an infinite medium (see Badr [22]). At the start of heating process, the heat is initially transferred from the inner wall through a very thin conduction layer, causing high heat transfer rate and so high \overline{Nu}_i values. The initial time stages are characterized by fast growth of the thermal layer resulting in a quick decrease in heat transfer rate. In these stages, the conduction heat transfer dominates

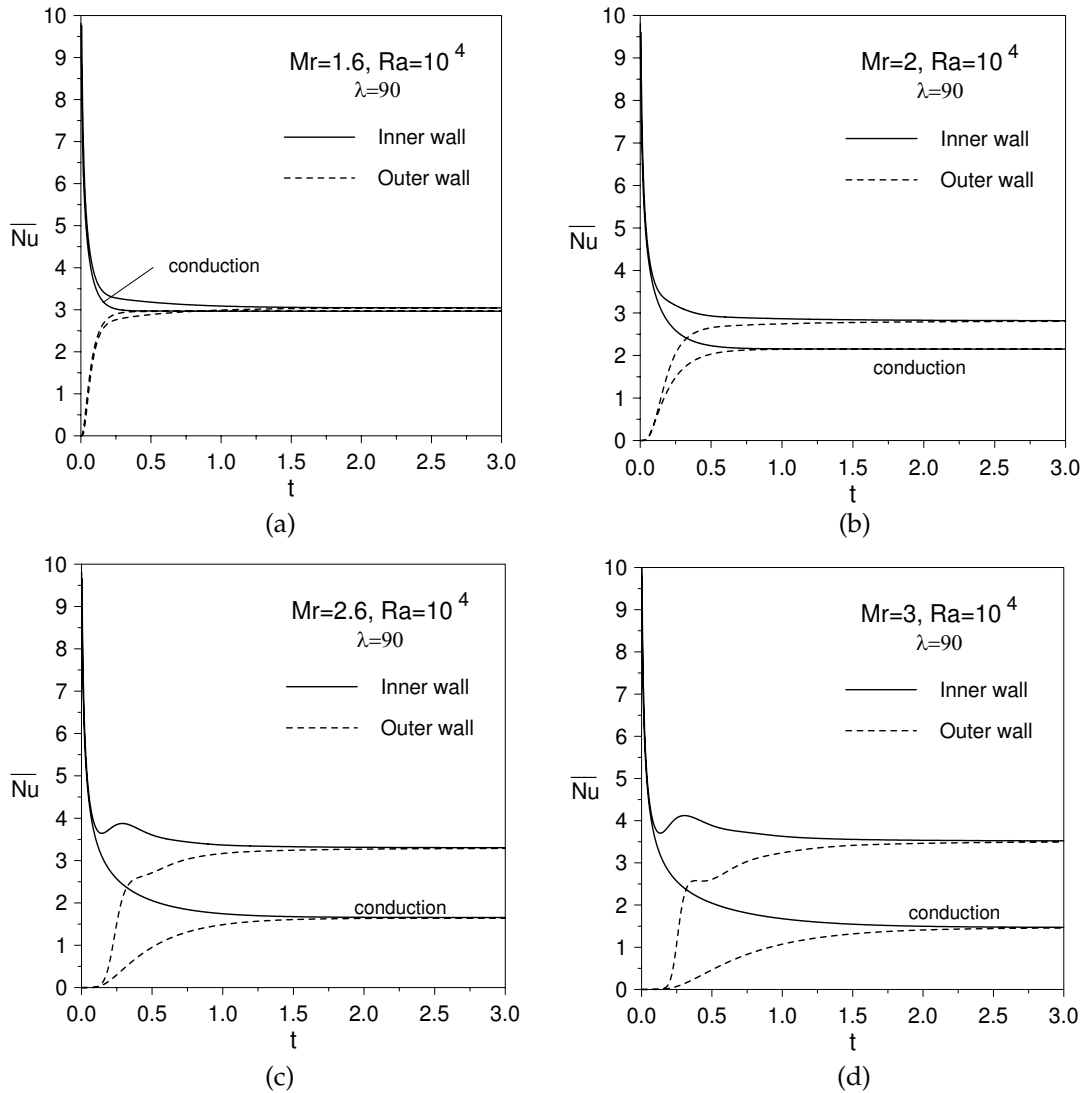


Figure 8: The time development of \overline{Nu} for inner and outer surfaces for the case of vertical annulus ($\lambda = 90$) and $Ra = 10^4$ and at different major axes ratios. (a) $Mr = 1.6$. (b) $Mr = 2$. (c) $Mr = 2.6$. (d) $Mr = 3$.

and the contribution of convection is almost negligible. This can be inferred from the coinciding of \overline{Nu} - t curve with that of conduction at these small times. Once the conduction thermal layer thickens enough, the convection starts effectively to take part in heat transfer process until the steady state is slowly approached. The steady state is reached when the rate of heat transfer from the inner surface is equal to that dissipated from the outer surface, thus satisfying the steady energy balance. When such steady state is reached, the Nusselt numbers at the inner and outer walls, \overline{Nu}_i and \overline{Nu}_o , will have the same value based on the present definitions. One more observation related to heat transfer from the inner surface is that for a relatively higher value of Mr ($Mr > 2$)

the transition from conduction dominated mode to convection dominated mode is accompanied with an overshoot in heat transfer rate and so an overshoot in \overline{Nu} (see Figs. 8c and 8d). This phenomenon is also reported in the case of transient heat convection from single isothermal elliptic or circular cylinder placed in infinite medium, see Ref. [19–23].

It is also clear from Figs. 8a-8d that the heat dissipated from the outer surface (and so \overline{Nu}_o) starts after a certain period of time delay. This period is actually the time needed to create a negative temperature gradient at the outer surface. Such temperature gradient takes place after the formation of a thermal fluid layer adjacent to that surface. That hot layer can exist due to either conduction diffusion or even through the circulating fluid heated by the inner surface. At small times, this hot circulating fluid is slow and gets cooled before reaching the outer surface resulting in zero temperature gradient and zero \overline{Nu}_o . As time increases, the hot thermal boundary layer is formed close to the outer surface and the heat from outer surface starts dissipating resulting in a continuous increase of \overline{Nu}_o until reaching steady state. The time delay for a given value of Ra depends on the annulus size and geometry. The narrower the annulus gap the smaller the time delay and vice versa. In case of a relatively narrow gap of $Mr=1.6$, the time delay is about 0.04 and increases to 0.13 for a gap with $Mr=2.0$ and further increases to 0.22 for gap of $Mr=2.6$ and for the widest gap considered in this study of $Mr=3$ it reaches 0.36. One can also observe from the figures that the time delay for this range of Mr is approximately equal to that of pure conduction or a bit smaller which means that the conduction diffusion mechanism is controlling this time delay period. For wider gaps, the delay period in the case of pure conduction is longer than that for the case of natural convection. The contribution of natural convection to steady heat transfer depends on the size of the annulus. The narrow annulus gaps hinder the convection currents and weaken heat convection. In these cases the heat transfer is mainly due to conduction. While in case of a relatively ample or wider annulus gaps the convection currents move freely and intensively, enhancing effectively the heat transfer process. The contribution of convection or the percentage increase of heat transfer due to convection in case of a narrow annulus gap (Fig. 8a) is about 3% in case of $Mr=1.6$ and about 50% in case of $Mr=2$. Such percentage increases significantly for a relatively wider annulus gap with an increase up to 90% in case of 2.6 and further up to 120% in case of $Mr=3$ (Fig. 8d).

The results obtained for the average Nusselt number for the cases considered at $Ra=10^4$ and $Ra=10^5$ and at different angles of inclination, λ , and major axes ratios, Mr , are shown in Table 1. It is clear from the table that \overline{Nu} increases with the increase of Ra for constant values of λ and Mr . However, for a narrower annulus gap with $Mr=1.2$, the conduction mode of heat transfer is very dominant and the effect of convection and so Ra and λ is negligible as can be observed in the table. One can also observe from Table 1 that the effect of angle of inclination, though not significant, is similar to that reported by Badr [22] for the case of an elliptic tube placed in an infinite medium. The obtained results indicate that at fixed values of Ra and Mr , \overline{Nu} increases with the increase of the angle of inclination from 0 to 90°. Table 1 also shows that for a

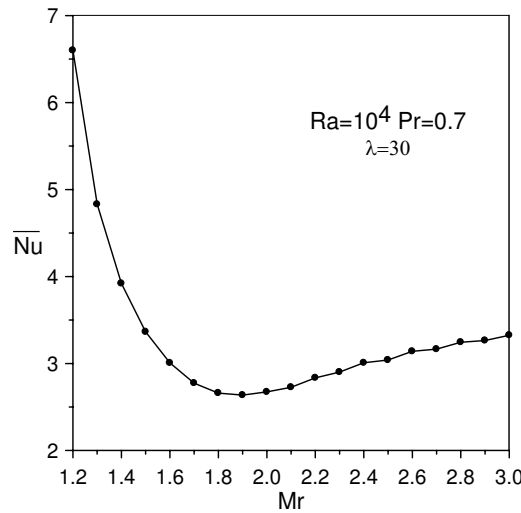


Figure 9: The average Nusselt number, \overline{Nu} variation with Mr for the case of 10^4 , $\lambda = 30$.

given angle, $\lambda=0$, \overline{Nu} reaches its minimum at $Mr=2.0$, for $Ra=10^4$ and at $Mr=1.6$ for $Ra=10^5$. This gives rise to the possibility of having a minimum value for Nu at a certain value of Mr for every value of Ra . In order to delineate this point some detailed calculations were carried out at $Ra=10^4$ and $\lambda=30^\circ$ with a step of 0.1 for Mr . The results which are presented in Fig. 9 clearly show that \overline{Nu} is minimum at $Mr=1.95$. The minimum value for \overline{Nu} , as can be inferred from the results, is Ra dependent; as Ra increases the value of Mr creating \overline{Nu}_{min} decreases. The existence of \overline{Nu}_{min} can be explained based on the fact that heat transfer from the inner surface is controlled by two mechanisms, namely, the conduction and convection modes. The effect of Mr on these two modes is different. As Mr increases, the conduction resistance increases and the conduction mode becomes less effective. On the other hand, the increase of Mr causes an increase in the convection currents and the convection mode becomes

Table 1: The average Nusselt number at $Ra = 10^4$ and $Ra = 10^5$ and at different Mr and λ .

Ra	λ	\overline{Nu}				
		$Mr=1.2$ (6.603)*	$Mr=1.6$ (2.971)*	$Mr=2.0$ (2.151)*	$Mr=2.6$ (1.652)*	$Mr=3$ (1.461)*
10^4	0	6.602	2.992	2.610	3.020	3.185
	30°	6.603	3.006	2.672	3.145	3.334
	60°	6.603	3.031	2.772	3.243	3.482
	90°	6.604	3.042	2.810	3.291	3.515
10^5	0	6.607	4.376	4.994	5.314	5.415
	30°	6.615	4.488	5.225	5.510	5.634
	60°	6.616	4.645	5.301	5.810	5.989
	90°	6.618	4.715	5.442	5.915	6.115

* steady \overline{Nu}_{cond} .

more effective. Therefore, as a result of increasing Mr the contribution of conduction gets lower while the contribution of convection gets higher. The opposite effect of the two mechanisms creates a minimum Nusselt number at a certain value of Mr for every value of Ra .

The effect of the major axis ratio, Mr , on the steady streamline and isotherm patterns is shown in Fig. 10 for the case of $Ra=10^4$ when the two major axes are horizontal ($\lambda=0$) while its effect on the local Nusselt number and vorticity distributions for the same case is shown in Figs. 11 and 12. Fig. 10 shows that for a narrow gap annulus ($Mr \leq 1.6$), the isotherms appear as almost concentric ellipses declaring the domination of the conduction mode. The fluid velocity in this case is low as a result of small average area of the annulus gap. Such low velocities can be inferred from the small values of the stream function. The local Nusselt number distribution along the outer surface, Fig. 11b, shows no significant variations along the surface. This again reflects the domination of conduction mode and the weak contribution of the convection mode. As the axis ratio increases to $Mr=2$, the annulus gap becomes wider and the fluid motion as appears from the higher values for stream function, becomes more noticeable with the centre of the two eddies moving up and with clear signs of developing a thermal plume at the top part of the annulus. As Mr increases further to $Mr=2.6$ and 3, the fluid circulation becomes more vigorous, leading to severe fluid impingement on the upper part of the annulus and more development of the thermal plume. The more intensive fluid motion is reflected as an increase of vorticity at all points on the

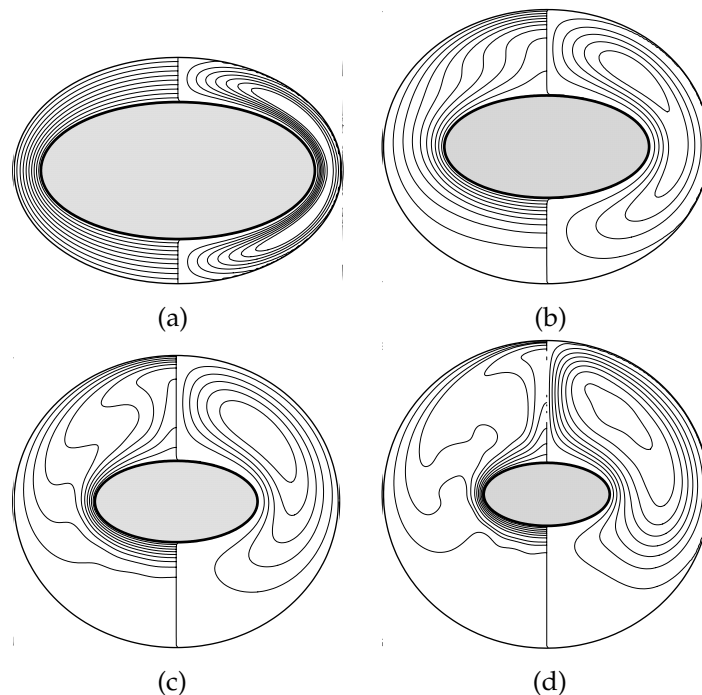


Figure 10: The patterns of flow and isotherms for the case of $Ra = 10^5$, $\lambda = 0$ and at different values of Mr . (a) $Mr = 1.2$. (b) $Mr = 1.6$. (c) $Mr = 2$. (d) $Mr = 2.6$.

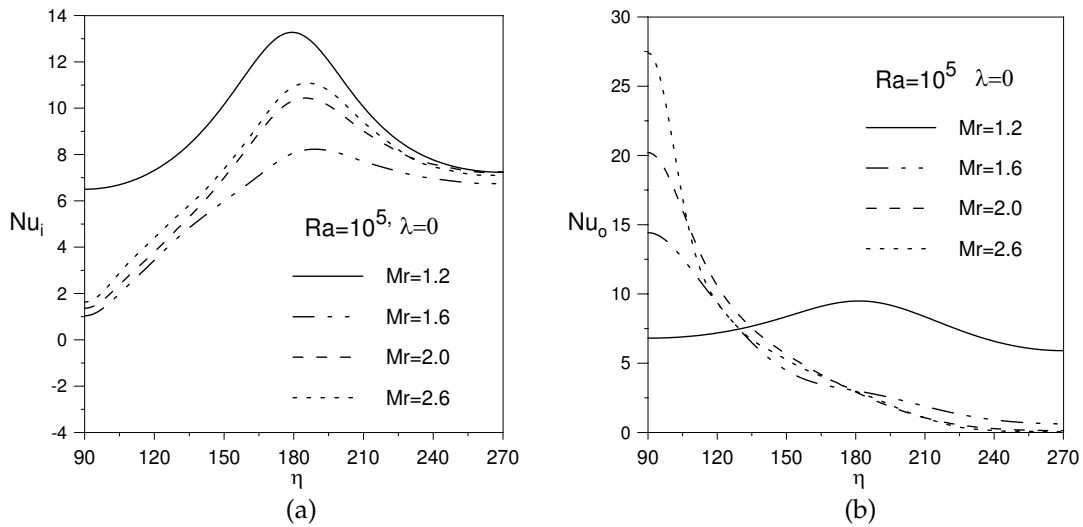


Figure 11: The local Nusselt number distribution along (a) the inner surface and along (b) the outer surface for the case $Ra = 10^4$, $\lambda = 0$ and different values of Mr .

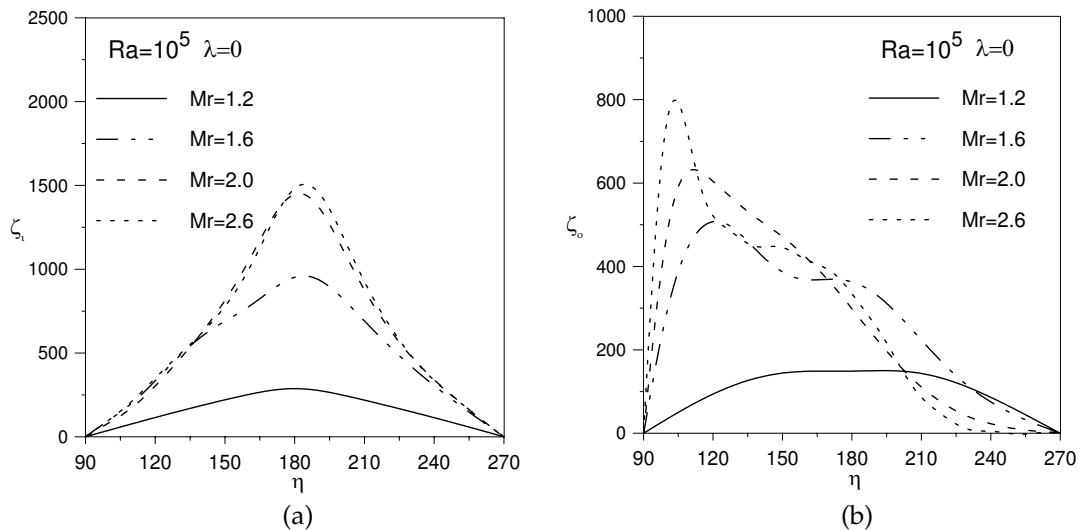


Figure 12: The vorticity distribution along (a) the inner surface and along (b) the outer surface for the case $Ra = 10^4$, $\lambda = 0$ and different values of Mr .

inner and outer surfaces as shown in Fig. 12a, b. This is accompanied by the development of the thermal plume in the upper part of the annulus resulting in an appreciable increase in Nu_o in that region.

Fig. 13 Shows the patterns of flow and isotherms for the case of $Ra=10^4$ and $Mr=2$ at different angle of inclination. It can be seen from the figure that the flow field still possesses two circulating eddies one on each side. These two eddies are no longer symmetric (except for $\lambda=0, 90^\circ$) but rather distorted. However, the flow along the

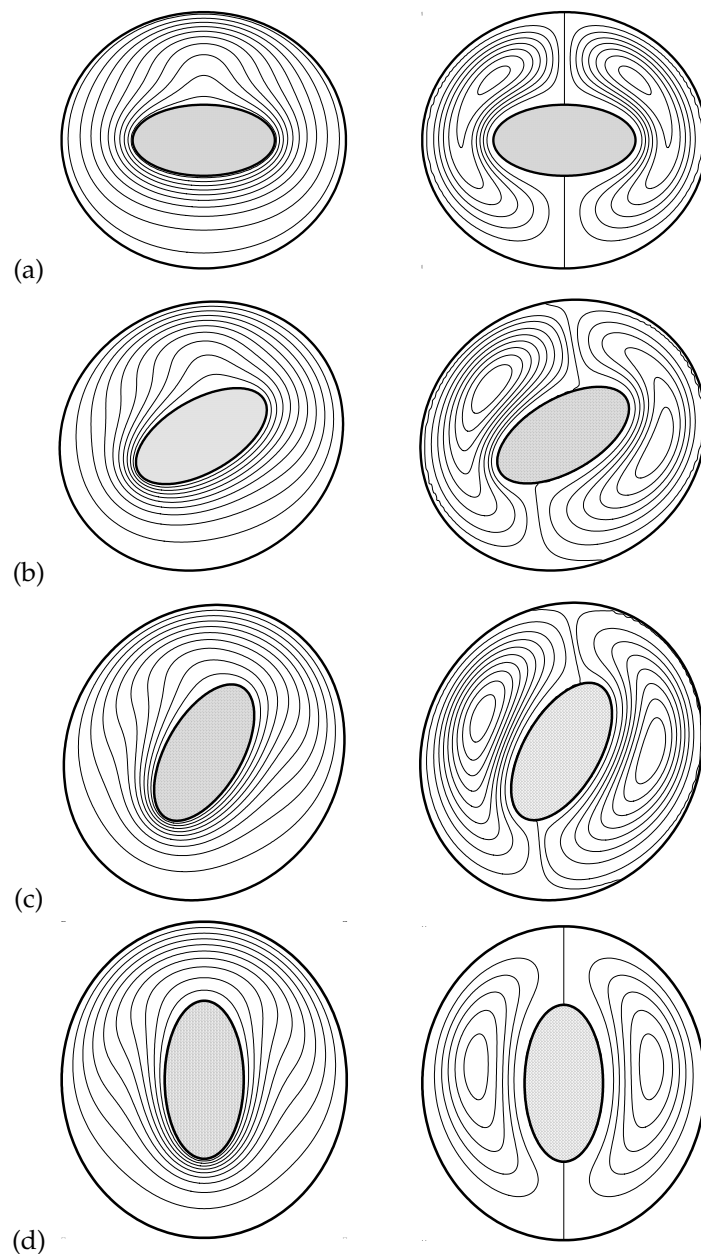


Figure 13: The patterns of streamlines (right) and isotherms (left) for the case of $Ra = 10^4$ and $Mr = 2$ and at different angle of inclination. (a) $\lambda = 0$. (b) $\lambda = 30$. (c) $\lambda = 60$. (d) $\lambda = 90$.

inner and outer surfaces is still having separation and stagnation points. The flow stagnates at the lower end of the inner surface and separates at the top part of the surface. While the flow stagnates at the top part of outer surface and separates from the lower part. The points of stagnation are usually the points of high Nu while that

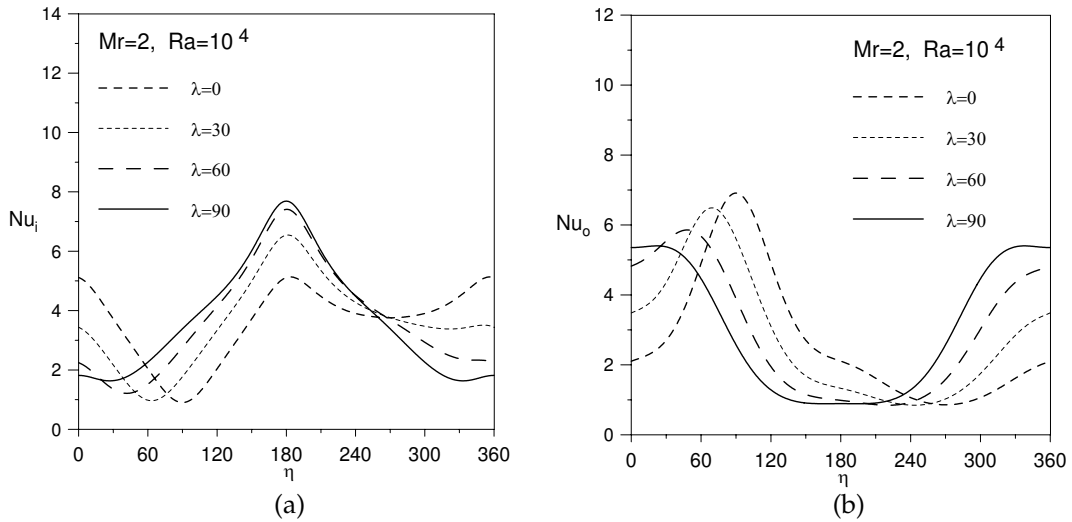


Figure 14: The local Nusselt number distribution along (a) the inner surface and along (b) the outer surface for the case $Ra = 10^4$, $\lambda = 0$ and different values of Mr .

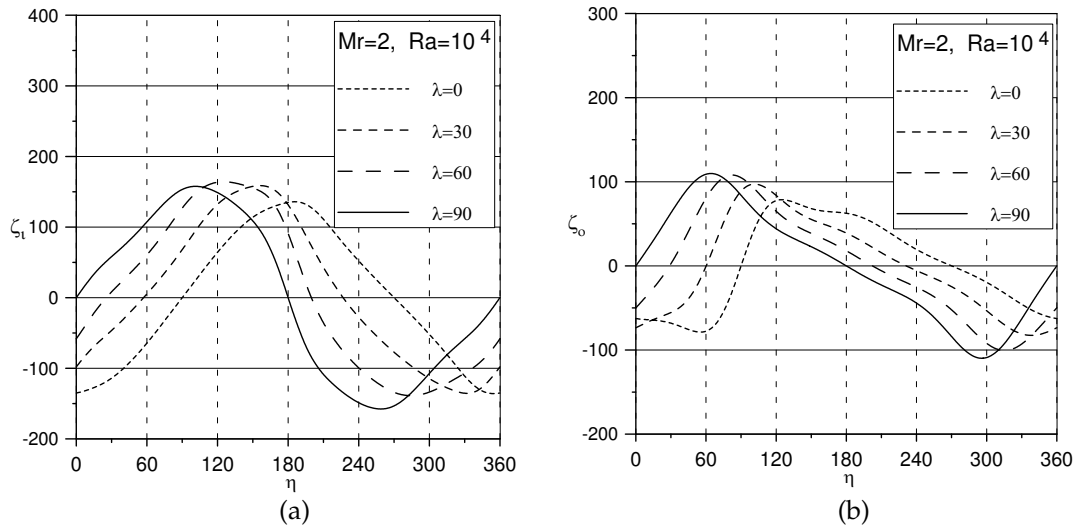


Figure 15: The vorticity distribution along (a) the inner surface and along (b) the outer surface for the case of $Ra = 10^4$, $Mr = 2$ at different angles of inclination.

of separation are the points of low Nu as shown in Fig. 14. The separation and stagnation points for the cases of inclined ellipses are no longer at 0 and 180° but rather deviates as shown in Fig. 14. In order to trace the points of separation and stagnation, the vorticity distribution on each surface is calculated and presented in Fig. 15. The points of zero vorticity at the wall are the points of either separation or stagnation. For the symmetrical cases (cases of $\lambda=0, 90^\circ$), the points of separation and stagnation are located on the vertical line of symmetry. For the case of $\lambda=30^\circ$, the separation

and stagnation points for the inner surface are respectively 58° and 227° while the separation and stagnation points for the outer surface are 60° and 231° . For the case of $\lambda=60^\circ$, these four points in sequence are 26° , 200° , 29° and 203° . The values of these points or angles simply tells approximately that the flow at the upper part of the annulus summon up vertically, regardless of inclination, forming a thermal plume in the vertical upper part of the annulus same as the case of symmetrical annulus. The effect is clear in Nu distribution on the outer surface where it can be seen that the Nu reaches maximum at the uppermost vertical point in all cases.

6 Conclusions

The problem of transient and steady natural convection in an elliptical annulus has been numerically investigated using the Fourier Spectral Method (FMS). The heat convection within the annulus is dependent on Rayleigh number, Prandtl numbers, angle of inclination of minor axes to gravity vector, ratio of outer tube major axis to inner tube major axis and the axes ratio of the inner tube. The results are obtained at two values of Rayleigh number of 10^4 and 10^5 . The major axes ratio is varied up to 3 while the angle of orientation of the minor axes is varied up to 90° . The Prandtl number and inner tube axis ratio are fixed at 0.7 and 0.5, respectively. The results for the special case of natural convection in concentric annulus are first obtained and compared with the earlier reported data and very good agreement has been found. The results for local and average Nusselt numbers are presented and discussed together with the details of both flow and thermal fields at various annulus orientations. The study has shown that at a certain Ra there is a value of the major axes ratio at which the heat transfer through the annulus reaches its minimum. This value decreases as Ra increases. The use of the Fourier Spectral Method in handling the present problem proves its success as a powerful numerical tool for solving confined heat convection/fluid flow associated problems.

Acknowledgments

The support received from Department of Mechanical Engineering, UET Taxila, Pakistan and from King Fahd University of Petroleum & Minerals, Dhahran, Saudi Arabia is very highly appreciated.

Appendix

Nomenclature

a_i	length of semi-major axis of inner tube
Ar_i	axis ratio of inner tube
Ar_o	axis ratio of outer tube

a_o	length of semi-major axis of outer tube
b_i	length of semi- minor axis of inner tube
b_o	length of semi-minor axis of outer tube
c	specific heat of the fluid
d'	ellipse eccentricity ($a_i = \sqrt{1 - Ar_i^2}$)
d	dimensionless ellipse eccentricity ($= d' / a_i$)
f_n, F_n	Fourier coefficients
F_b	buoyancy force
g	gravitational acceleration
g_n, G_n	Fourier coefficients
h, \bar{h}	local and average heat transfer coefficients
h_n, H_n	Fourier coefficients
J	Jacobian of coordinate transformation
k	thermal conductivity
Mr	major axes ratio ($= a_o / a_i$)
Nu, \bar{Nu}	local and average Nusselt numbers
Pr	Prandtl number ($= \nu / \alpha$)
Ra	Rayleigh number ($= g\beta(2a_i)^3(T_s - T_\infty) / \alpha\nu$)
t	dimensionless time
T	temperature
x', y'	Cartesian coordinates
x, y	dimensionless Cartesian coordinates
X^*	the distance from inner tube surface along line $\eta = 0$, ($= (x' - a_i) / (a_o - a_i)$)
Y^*	the distance from inner tube surface along line $\eta = 90$, ($= (y' - b_i) / (b_o - b_i)$)

Greek symbols

α	thermal diffusivity
β	coefficient of thermal expansion
ϕ	dimensionless temperature = $(T - T_o)(T_i - T_o)$
η, ξ	elliptical coordinates
λ	annulus major axes angle of inclination to the horizontal
ν	kinematics viscosity
ρ	density
τ	time
ψ', ψ	dimensional and dimensionless stream functions
ζ', ζ	dimensional and dimensionless vorticity

Subscripts

i	at the inner tube surface
o	at the outer tube surface

References

- [1] T. H. KUEHN AND R. J. GOLDSTEIN, *An experimental and theoretical study of natural convection in the annulus between horizontal concentric cylinders*, J. Fluid Mech., 74 (1976), pp. 695–719.
- [2] T. H. KUEHN AND R. J. GOLDSTEIN, *An experimental study of natural convection heat transfer in concentric and eccentric horizontal cylindrical annuli*, ASME, J. Heat Transfer, 100 (1978), pp. 635–640.
- [3] U. PROJAHN, H. RIEGER AND H. BEER, *Numerical analysis of laminar natural convection between concentric and eccentric cylinders*, Numer. Heat Transfer, 4 (1981), pp. 131–146.
- [4] C. H. CHO, K. S. CHANG AND K. H. PARK, *Numerical simulation of natural convection in concentric and eccentric horizontal annuli*, ASME, J. Heat Transfer, 104 (1982), pp. 624–630.
- [5] H. M. BADR, *Study of laminar free convection between two eccentric horizontal tubes*, T. Can. Soc. Mech. Eng., 7 (1983), pp. 191–198.
- [6] D. W. PEPPER AND R. E. COOPER, *Numerical solution of natural convection in eccentric annulus*, AIAA J., 21 (1983), pp. 1331–1337.
- [7] J. PRUSA AND L. S. YAO, *Natural convection heat transfer between eccentric horizontal cylinders*, ASME, J. Heat Transfer, 105 (1983), pp. 108–116.
- [8] D. NAYLOR, H. M. BADR AND J. D. TARASUK, *Experimental and numerical study of natural convection between two eccentric tubes*, Int. J. Heat Mass Transfer, 32 (1989), pp. 171–181.
- [9] G. GUJ AND F. STELLA, *Natural convection in horizontal eccentric annuli: numerical study*, Numer. Heat Transfer, 27 (1995), pp. 89–105.
- [10] C. SHU, Q. YAO AND K. S. YEO, *An efficient approach to simulate natural convection in arbitrarily eccentric annuli by vorticity-stream function formulation*, Numer. Heat Transfer, A 38 (2000), pp. 739–756.
- [11] J. H. LEE AND T. S. LEE, *Natural convection in the annuli between horizontal confocal elliptic cylinders*, Int. J. Heat and Transfer, 24 (1995), pp. 1739–1742.
- [12] M. M. ELSHAMY, M. N. OZISIK AND J.P. COULTER, *Correlation for laminar natural convection between confocal horizontal elliptical cylinders*, Numer. Heat Transfer, A 18 (1990), pp. 95–112.
- [13] C. H. CHENG AND C. C. CHAO, *Numerical prediction of the buoyancy driven flow in the annulus between horizontal eccentric elliptical cylinders*, Numer. Heat Transfer, A 30 (1996), pp. 283–303.
- [14] Y. D. ZHU, C. SHU, J. QIU AND J. TANI, *Numerical simulation of natural convection between two elliptical cylinders using DQ method*, Int. J. Heat and Transfer, 47 (2004), pp. 797–808.
- [15] W. C. SCHREIBER AND S. N. SINGH, *Natural convection between confocal horizontal elliptical cylinders*, Int. J. Heat and Mass Transfer, 28 (1985), pp. 807–822.
- [16] H. M. BADR AND S. C. R. DENNIS, *Time-dependent viscous flow past an impulsively started rotating and translating circular cylinder*, J. Fluid Mech., 158 (1985), pp. 447–488.
- [17] F. M. MAHFOUZ AND H. M. BADR, *Flow structure in the wake of a rotationally oscillating cylinder*, ASME J. Fluid. Eng., 122 (2000), pp. 290–301.
- [18] U. GRIGULL AND W. HAUF, *Natural convection in horizontal cylindrical annuli*, Int. Heat Transfer Conf. Chicago, 3 (1966), pp. 183–195.
- [19] J. R. PARSONS JR. AND J. C. MULLGAN, *Transient free convection from a suddenly heated horizontal wire*, ASME, J. of Heat Transfer, 100 (1978), pp. 423–428.
- [20] H. M. BADR, *Heat transfer in transient buoyancy driven flow adjacent to a horizontal rod*, Int. J Heat and Mass Transfer, 30 (1987), pp. 1990–2012.
- [21] P. WANG, R. KAHAWITA AND D. L. NGUYEN, *Transient laminar convection from horizontal*

- cylinders*, Int. J. Heat and Mass Transfer, 34 (1991), pp. 1429–1442.
- [22] H. M. BADR, *Laminar natural convection from elliptic tube with different orientations*, ASME, J. Heat Transfer, 119 (1997), pp. 709–718.
- [23] F. M. MAHFOUZ, *Transient free convection from a horizontal cylinder placed in a micropolar fluid*, Heat and Mass Transfer, 39 (2003), pp. 455–462.